Microstructural Development and Catalytic Performance of Au−Pd Nanoparticles on Al_2O_3 Supports: The Effect of Heat Treatment Temperature and Atmosphere

A. A. Herzing,*[,†,‡] A. F. Carley,[§] J. K. Edwards,[§] G. J. Hutchings,[§] and C. J. Kiely[†]

Center for Advanced Materials and Nanotechnology, Lehigh University, 5 East Packer Avenue, Bethlehem, Pennsylvania 18015-3195, National Institute of Standards and Technology, 100 Bureau Drive, Gaithersburg, Maryland 20899, and School of Chemistry, Cardiff University, Main Building, Park Place, Cardiff CF10 3AT, U.K.

Received September 26, 2007. Revised Manuscript Received December 3, 2007

Au−Pd nanoparticles supported on a variety of oxides are known to be highly active catalysts for a number of interesting reactions, including the direct synthesis of H_2O_2 from H_2 and O_2. A systematic series of Au−Pd/Al_2O_3 catalysts, subjected to a variety of heat treatments, have been examined by STEM-XEDS and XPS in an effort to track the microstructural development of the bimetallic particles. It was observed that the nature and size distribution of the AuPd particles was highly dependent upon both the heat treatment temperature and the atmosphere. As synthesized particles were homogeneous alloys, but subsequent calcination in air produced metal particles which showed a progressive enrichment of Pd at their surface. The change from homogeneous alloy to Pd-rich shell/Au-rich core morphology and increase in average particle size induced by the calcination treatment was accompanied by a significant decrease in the activity of the catalyst. However, the calcination step is deemed to be necessary to produce a stable reusable catalyst that resists leaching of the metal from the oxide surface into solution. Furthermore, it is shown that the subsequent reduction of a previously calcined catalyst is highly deleterious to its performance and stimulates many of the AuPd particles to "invert" and form a Pd-rich core/Au-rich shell morphology.

1. Introduction

Hydrogen peroxide (H_2O_2) is used on a large scale in industry as a bleaching agent and a disinfectant. From a green chemistry standpoint, H_2O_2 is a nearly ideal oxidizing agent because the primary byproduct formed during such reactions is water. However, the H_2O_2 synthesis process has recently become the subject of renewed scrutiny, because the standard production route is an indirect process involving the sequential hydrogenation and oxidation of alkyl anthraquinone.[1] This indirect process has several environmental drawbacks and only becomes cost-effective at a very large scale, and, thus, the synthesis, transportation, and storage of large amounts of H_2O_2 becomes necessary.

A direct production route involving the reaction of gaseous H_2/O_2 mixtures would be preferable for applications where H_2O_2 is only required in small amounts and could be made "on site", such as in the fine chemicals industry or remote field hospitals. Pd catalysts have been extensively studied for this direct combination reaction and have been shown to produce significant amounts of H_2O_2.[2–9] While early studies using this type of catalyst were carried out using mixtures of H_2 and O_2 in the explosive regime, more recent work has proved successful in operating under safer conditions using dilute H_2/O_2 solutions.[2,4,10,11]

There is an intrinsic difficulty in achieving significant H_2O_2 production because the subsequent back-transformation of H_2O_2 to water via hydrogenation and/or decomposition proceeds readily at low temperature because the heats of reaction for these two deleterious processes (−211.5 and −105.8 kJ/mol, respectively) are quite similar to that of the direct combination reaction (−135.9 kJ/mol).[12] Hutchings and co-workers[12,13] have reported the coimpregnation of Al_2O_3 support particles with both Pd and Au produced catalysts that were significantly more active for the direct synthesis of H_2O_2 from molecular H_2 and O_2 than either of their pure-metal counterparts. The metal particles in this case

* Corresponding author. E-mail: andrew.herzing@nist.gov. Tel.: (301) 975-2860. Fax: (301) 417-1321.
† Lehigh University.
‡ National Institute of Standards and Technology.
§ Cardiff University.

(1) Hess, H. T. *Kirk-Othmer Encyclopaedia of Chemical Technology*; Wiley: New York, 1995; Vol. 13, p 961.
(2) Van Weynbergh, J.; Schoebrechts, J.-P.; Chaumont-Gistoux, J.-C. U.S. Patent 5447706, 1995.
(3) Henkel, H.; Weber, W. U.S. Patent 1108752, 1914.
(4) Zhou, B.; Lee, L.-K. U.S. Patent 6168775, 2001.
(5) Gosser, L. W.; Schwartz, J. -A. T. U.S. Patent 4772458, 1988.
(6) Choudhary, V. R.; Sansare, S. D.; Gaikwad, A. G. *Catal. Lett.* **2002**, *84*, 81.
(7) Choudhary, V. R.; Samanta, C.; Gaikwad, A. G. *Chem. Comm.* **2004**, *18*, 2004.
(8) Dissanayake, D.; Lunsford, J. *J. Catal.* **2002**, *206*, 173.
(9) Dissanayake, D.; Lunsford, J. *J. Catal.* **2003**, *214*, 113.
(10) Gaikwad, A. G.; Sansare, S. D.; Choudhary, V. R. *J. Mol. Catal. A: Chem.* **2002**, *181*, 143.
(11) Melada, S.; Rioda, R.; Menegazzo, F.; Pinna, F.; Strukul, G. *J. Catal.* **2006**, *239*, 422.
(12) Landon, P.; Collier, P. J.; Papworth, A. J.; Kiely, C. J.; Hutchings, G. J. *Chem. Commun.* **2002**, 2058.
(13) Landon, P.; Collier, P. J.; Papworth, A. J.; Kiely, C. J.; Hutchings, G. J.; Burrows, A. *Phys. Chem. Chem. Phys.* **2003**, *5*, 1917.

10.1021/cm702762d CCC: $40.75
Published on Web 01/25/2008

were found to be alloys of Au and Pd that existed over a wide range of compositions despite having a nominal Au: Pd weight ratio of 1:1. Subsequent work using similar Au−Pd bimetallic catalysts[14–18] has further demonstrated the synergistic effect of simultaneously using Au *and* Pd supported on a variety of materials (e.g., TiO_2, Fe_2O_3, Al_2O_3) for the directed combination reaction as well as the selective oxidation of alcohols to aldehydes.[19] The origin of the enhanced performance of supported Pd catalysts via the addition of Au has been suggested to arise from both structural[20] and electronic[21] alterations in the nature of the metal particle surfaces.

In the present work, we build upon our previously reported results[15] which showed that calcination at elevated temperature of oxide-supported Au−Pd catalysts was necessary to prevent catalyst degradation during use. Even though the fresh, uncalcined material exhibited a significantly higher degree of H_2O_2 production, the metal was easily leached from the support surface into the reactant solution, which caused the catalytic performance to decrease upon reuse. Extensive characterization of such catalysts via scanning transmission electron microscopy (STEM) and X-ray photoelectron spectroscopy (XPS) suggested that the surfaces of the metal alloy particles were significantly enriched with Pd during the calcination treatment, producing particles with a Au-rich core/Pd-rich shell morphology.[14–19] To more fully understand the development of this surface enrichment and its effect on catalytic performance, a systematic study has been undertaken of a series of Au−Pd/Al_2O_3 catalysts subjected to various heat treatments so that the morphological changes could be systematically monitored in the bimetallic particles and correlated with the resulting catalytic performance.

2. Experimental Section

2.1. Catalyst Preparation. A series of Au−Pd/Al_2O_3 catalysts were prepared by impregnation of γ-Al_2O_3 (Condea SCF-140) via an incipient wetness method using aqueous solutions of $PdCl_2$ (Johnson Matthey) and $HAuCl_4 \cdot 3H_2O$ (Johnson Matthey). The detailed procedure was as follows: an aqueous solution (10 mL) of $HAuCl_4 \cdot 3H_2O$ (5 g in 250 mL of water) and an aqueous $PdCl_2$ solution (4.15 mL of a solution of 1 g of $PdCl_2$ in 25 mL of water) were simultaneously added to γ-alumina (3.8 g). The paste formed was ground and dried at 120 °C for 16 h. Subsequently, this precursor material was thermally treated under a range of conditions: calcination in static air at 200 °C for 4 h; calcination in static air at 400 °C for 4 h; and calcination in static air at 400 °C for 4 h followed by reduction in flowing H_2 (5 wt % H_2 in Ar) at 500 °C for 5 h. All materials were used fresh; that is, they were catalytically tested within a few hours of synthesis.

2.2. Catalyst Testing. Hydrogen peroxide synthesis was performed using a Parr Instruments stainless steel autoclave with a nominal volume of 50 mL and a maximum working pressure of 14 MPa. The autoclave was equipped with an overhead stirrer (0–2000 rpm) and provision for measurement of temperature and pressure. Typically, the autoclave was charged with catalyst (0.01 g unless otherwise stated) and solvent (5.6 g of MeOH and 2.9 g of H_2O) purged three times with CO_2 (3 MPa) and then filled with 5% H_2/CO_2 and 25% O_2/CO_2 to give a hydrogen to oxygen ratio of 1: 2, at a total pressure of 3.7 MPa at 2 °C. Stirring (1200 rpm unless otherwise stated) was started on reaching the desired temperature, and experiments were run for 30 min unless otherwise stated. H_2O_2 yield was determined by titration of aliquots of the final filtered solution with acidified $Ce(SO_4)_2$ (7×10^{-3} mol/L). $Ce(SO_4)_2$ solutions were standardized against $(NH_4)_2Fe(SO_4)_2 \cdot 6H_2O$ using ferroin as indicator.

2.3. Catalyst Characterization. Samples were prepared for STEM examination by dispersing the catalyst powder in high purity ethanol and then allowing a drop of the suspension to evaporate on a holey carbon film supported by a 300 mesh copper TEM grid. High-angle annular dark-field (HAADF) imaging was carried out to determine particle size distributions in all catalysts using a JEOL 2200FS TEM/STEM equipped with a CEOS spherical aberration corrector. Annular dark-field (ADF) STEM imaging and elemental mapping via X-ray energy dispersive spectroscopy (XEDS) was carried out using a VG systems HB603 dedicated STEM operating at 300 kV equipped with a Nion spherical aberration corrector. The latter instrument was also fitted with an Oxford Instruments INCA TEM 300 system for X-ray spectrum image acquisition. Subsequent statistical processing of the XEDS spectrum image data obtained was carried out via multivariate statistical analysis (MSA) using the MSAXESP v. 0.11 code.[22] MSA is a specialized set of processing techniques that analyzes the spectrum image data cube as a whole and identifies the independently varying components it contains, thus allowing a significant reduction in the inherent background signal from the processed data.[23] Watanabe and co-workers[24,25] have shown that the application of MSA to STEM-XEDS spectrum imaging can significantly improve the quality and interpretability of the acquired data.

XPS spectra were measured on a Kratos Axis Ultra DLD spectrometer using a monochromatic Al Kα X-ray source (75 W) and an analyzer pass energy of 160 eV (survey scans) or 40 eV (detailed scans). Samples were mounted using double-sided adhesive tape, and binding energies are referenced to the C(1s) binding energy of adventitious carbon contamination taken to be 284.7 eV.

Atomic absorption spectroscopy (AAS) was performed with a Perkin-Elmer 2100 atomic absorption spectrometer using an air−acetylene flame. Gold/palladium samples were run at wavelengths 242.8 nm (Au) and 247.6 nm (Pd). Samples for analysis were prepared by dissolving 0.1 g of the dried catalyst in an aqua regia solution, followed by the addition of 250 mL deionized water to dilute the sample. AAS was used to determine the wt % of the metal incorporated onto the support after impregnation, as well as the concentration (ppm) of Au or Pd that had leached out into solution during reaction. This latter was deduced by determining

(14) Edwards, J. K.; Landon, P.; Carley, A. F.; Herzing, A. A.; Watanabe, M.; Kiely, C. J.; Hutchings, G. J. *J. Mater. Res.* **2007**, *22*, 831.
(15) Edwards, J. K.; Solsona, B. E.; Landon, P.; Carley, A. F.; Herzing, A.; Kiely, C. J.; Hutchings, G. J. *J. Catal.* **2005**, *236*, 69.
(16) Edwards, J. K.; Solsona, B. E.; Landon, P.; Carley, A. F.; Herzing, A.; Watanabe, M.; Kiely, C. J.; Hutchings, G. J. *J. Mater. Chem.* **2005**, *15*, 4595.
(17) Edwards, J. K.; Solsona, B. E.; Landon, P.; Carley, A. F.; Herzing, A.; Kiely, C. J.; Hutchings, G. J. *Chem. Mater.* **2006**, *18*, 2690.
(18) Edwards, J. K.; Carley, A. F.; Herzing, A. A.; Kiely, C. J.; Hutchings, G. J. *Faraday Discuss.* **2008**, in press.
(19) Enache, D. I.; Edwards, J. K.; Landon, P.; Solsona-Espriu, B.; Carley, A. F.; Herzing, A. A.; Watanabe, M.; Kiely, C. J.; Knight, D. W.; Hutchings, G. J. *Science* **2006**, *311*, 362.
(20) Chen, M. S.; Kumar, D.; Yi, C. W.; Goodman, D. W. *Science* **2005**, *310*, 291.
(21) Han, Y.-F.; Zhong, Z.; Ramesh, K.; Chen, F.; Chen, L.; White, T.; Tay, Q.; Yakkub, S. N.; Wang, Z. *J. Phys. Chem. C* **2007**, *111*, 8410.
(22) Watanabe, M. *MSAXESP*, version 0.11; National Center for Electron Microscopy, 2005 (beta).
(23) Trebbia, P.; Bonnet, N. *Ultramicroscopy* **1990**, *34*, 165.
(24) Burke, M. G.; Watanabe, M.; Williams, D. B.; Hyde, J. M. *J. Mater. Sci.* **2006**, *41*, 4512.
(25) Herzing, A. A.; Watanabe, M.; Edwards, J. K.; Conte, M.; Tang, Z.-R.; Hutchings, G. J.; Kiely, C. J. *Faraday Discuss.* **2008**), in press.

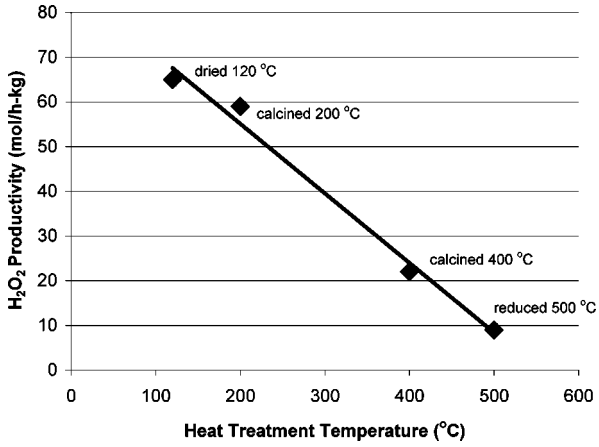

Figure 1. Hydrogen peroxide productivity of the Au−Pd/Al_2O_3 catalysts as a function of heat treatment.

the residual Au and Pd content of the used catalyst and comparing it with that of the fresh catalyst.

3. Results

3.1. Catalytic Testing and Catalyst Stability. After synthesis and respective heat treatments, the four samples were tested for their ability to catalyze the direct formation of H_2O_2 under identical conditions and produced very similar results to those reported previously.[15–17] Figure 1 shows that the H_2O_2 productivity, which was highest for the uncalcined sample (65 mol/(h·kg)), progressively decreased as the calcination temperature was increased from 200 °C (59 mol/(h·kg)) to 400 °C (22 mol/(h·kg)). Finally, subsequent reduction of the 400 °C calcined sample deactivated the material even further, yielding a productivity of only 9 mol/(h·kg).

However, despite the uncalcined catalyst exhibiting the highest productivity, it was found to be particularly unstable during a subsequent repeat cycle of catalytic tests because of leaching of the metal from the Al_2O_3 support into solution. It was found that, while the sample calcined at 400 °C is stable upon reuse, the productivity of the uncalcined catalyst drops by 36% to 42 mol/(h·kg) upon reuse. AAS analysis of the reactant solution after testing showed that 75% of the Au and 79% of the Pd had been leached from the uncalcined catalyst during the first reaction run. Similarly, analysis of the reactant stream after the uncalcined catalyst was reused showed that 80% of the remaining Au and 85% of the remaining Pd was leached from the catalyst during the second reaction run. By comparison, no detectable Au or Pd was leached from the 400 °C calcined catalyst during either reaction runs, thus explaining its stable catalytic performance. Very similar observations for titania supported Au−Pd catalysts were confirmed by XPS analysis of the catalyst samples.[15] Therefore, despite its superior catalytic performance in the initial test, the 120 °C catalyst must be calcined to improve its stability, even at the expense of losing some of its high productivity.

3.2. XPS Analysis of the Au−Pd/Al_2O_3 Catalysts. The valence state and physical dispersion of the Au and Pd in the four Au−Pd/Al_2O_3 samples was probed using XPS analysis. Figure 2 shows a comparison of the Au(4f) and Pd(3d) spectra recorded for the four samples. The spectra have been scaled according to the relative intensities of the Al(2p) signal from the Al_2O_3 support.

In the Au(4f) spectra (Figure 2a), the dried sample exhibits a significant chemical shift with respect to metallic gold, indicative of the presence of oxidized Au species. Furthermore, the large full width at half-maximum (fwhm) and peak shape suggest that both Au^{3+} and Au^{+} (or Au^{x+} and Au^0) are present; however, deconvolution of these peaks for quantitative analysis was not possible. For the sample calcined at 200 °C, the peaks shift to lower binding energy and become asymmetric, suggesting partial reduction to Au^0 of approximately 12% of the oxidized Au species. After the calcination treatment at 400 °C, a peak structure characteristic of metallic Au^0 is observed. Heating to 400 °C also results in a significant decrease in the Au(4f) intensity, suggesting that sintering of the metal particles has occurred during the calcination treatment. No change in the Au oxidation state occurs during the postcalcination reduction treatment at 500 °C, such that the Au remains fully reduced as expected. Finally, compared to the similar data discussed previously from the sample calcined at 400 °C, the Pd intensity has decreased significantly while the Au signal is more intense following reduction. At the very least, this suggests that the degree of Pd-surface enrichment is no longer as extreme as that observed in the sample which was only calcined.

The spectral region corresponding to the Pd(3d) and Au(3d) signal, shown in Figure 2b, provides evidence for Au depletion from the surface region after calcination. This is indicated by the significant decrease in the intensity of the Au($3d_{3/2}$) feature at 354 eV with increasing heat treatment temperature. Supporting Information Table 1 shows the Pd/Au ratio as deduced from the Pd(3d) and Au(4f) spectra, using Wagner's sensitivity factors, in which a clear increase in relative Pd concentration with increasing calcination temperature is evident.

For the dried catalyst and those materials calcined at 200 and 400 °C the Pd($3d_{5/2}$) binding energy is characteristic of Pd^{2+}, suggesting that the Pd is present as $PdCl_2$ and/or PdO. Most likely, in the uncalcined sample $PdCl_2$ is the most prevalent species which is then converted to PdO upon heat treatment. However, difficulty exists in determining when this conversion takes place because of the presence of residual Cl on the support surface in all of the samples (see Supporting Information Table 1). After reduction at 500 °C, the peak decreases in intensity and shifts approximately 2 eV to lower binding energy consistent with a transformation to Pd^0. However, the peak is asymmetric, exhibiting a shoulder at even higher binding energy, suggesting that some surface oxide layer component persists even after the reduction treatment.

3.3. Aberration-Corrected STEM Analysis of the Au−Pd/Al_2O_3 Catalysts. *3.3.1. Particle Size Determination via HAADF Imaging.* Aberration-corrected STEM-HAADF imaging was utilized to determine the size distribution of metal particles contained in the set of Au−Pd/Al_2O_3 catalysts. As shown in Figure 3a,b the uncalcined catalyst was found to exhibit a bimodal distribution of particle sizes, with the smaller, far more plentiful particles ranging from 0.5–2 nm

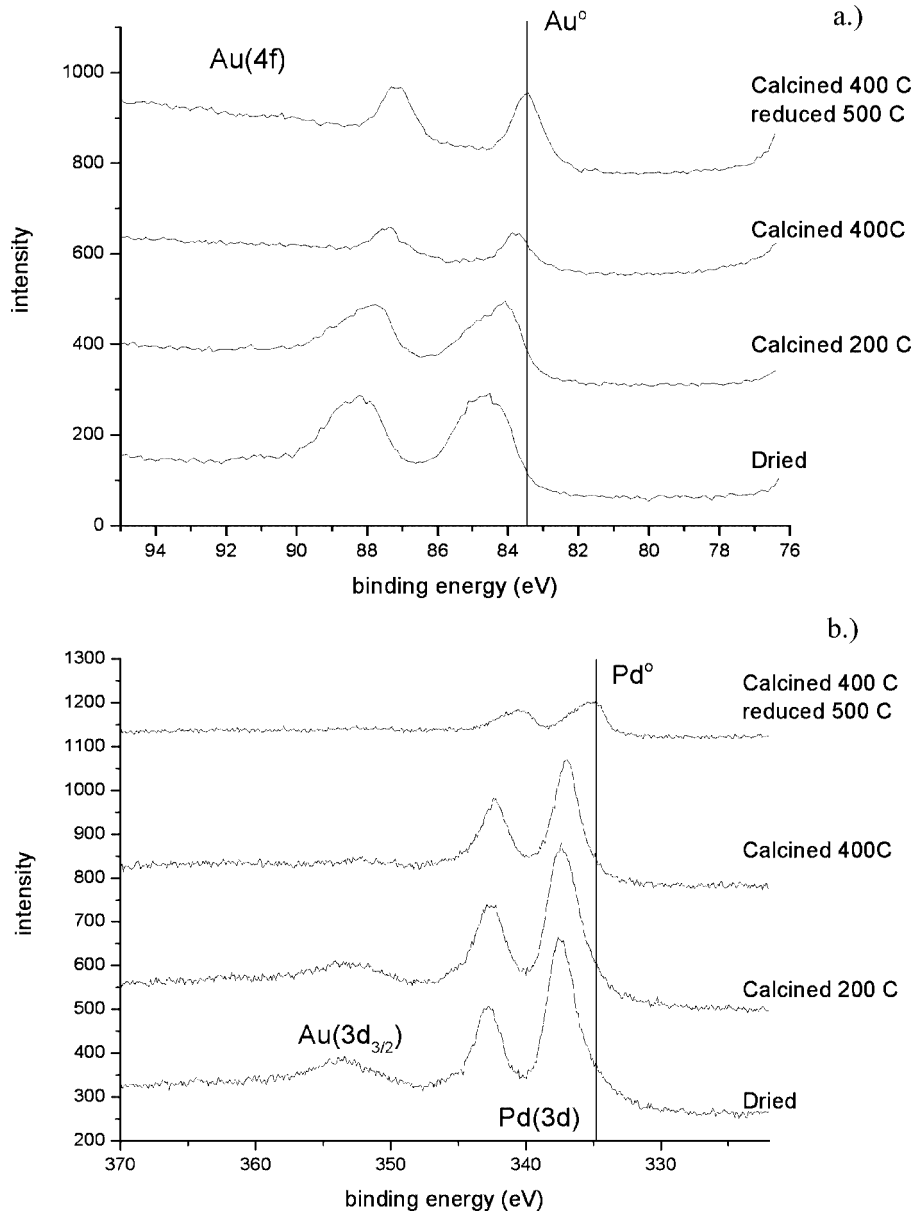

Figure 2. XPS spectra of the (a) Au(4f) and (b) Pd(3d) peaks in the dried, calcined, and reduced Au−Pd/Al_2O_3 catalysts. Sintering of the metal particles is indicated by the decrease in overall Au(4f) signal, and reduction of the Au^+ to Au^0 is evidenced by the shift of the peaks to lower binding energies. Note the disappearance of the $Au(3d_{3/2})$ signal upon calcination indicating the development of a Au−Pd core–shell structure.

Table 1. Summary of Heat Treatment Conditions Used To Synthesize the Au−Pd/Al_2O_3 Catalysts and Pd/Au Ratios As Determined via XPS Analysis[a]

treatment	molar Pd/Au ratio	Pd:Au ratio by weight
dried at 120 °C	1.4	0.8
calcined at 200 °C[b]	2.1	1.5
calcined at 400 °C[b]	9.1	4.9
calcined at 400 °C and then reduced at 500 °C[b,c]	6.0	3.2

[a] All samples contained 2.5wt.%Au and 2.5wt.% Pd as determined by AAS. [b] Calcination treatments were carried out in air for 4 h. [c] Reduction treatment was carried out in flowing H_2 (5 wt.% in Ar) for 5 h.

in size and the larger, and considerably rarer, particles being 10–50 nm in size. As shown in the images, these latter particles are very much in the minority, representing less than 1% of the total number of particles. It is interesting to note the presence of such occasional larger particles in the catalyst prior to calcination, which suggests that they are an inherent byproduct of the impregnation process and are not formed exclusively via the high-temperature sintering processes.

After calcination at 200 °C (Figure 3c,d) a broader trimodal particle size distribution developed that consisted of the small (2 nm and less) and a tiny number of the larger (10–50 nm; not shown) particles noted in the uncalcined catalyst. In addition, intermediate sized particles (2–5 nm) were also detected in this sample which were not observed in the precursor material, and this implies that sintering of many of the smallest particles had occurred during the 200 °C calcination treatment.

Upon calcination at 400 °C, the number density of the larger 10–50 nm particles increases significantly (Figure 3e,f), while the population of the 0.5–2 nm particles dramatically decreased. Instead, nearly all of the metal is now contained within particles that are between 2 and 5 nm in diameter.

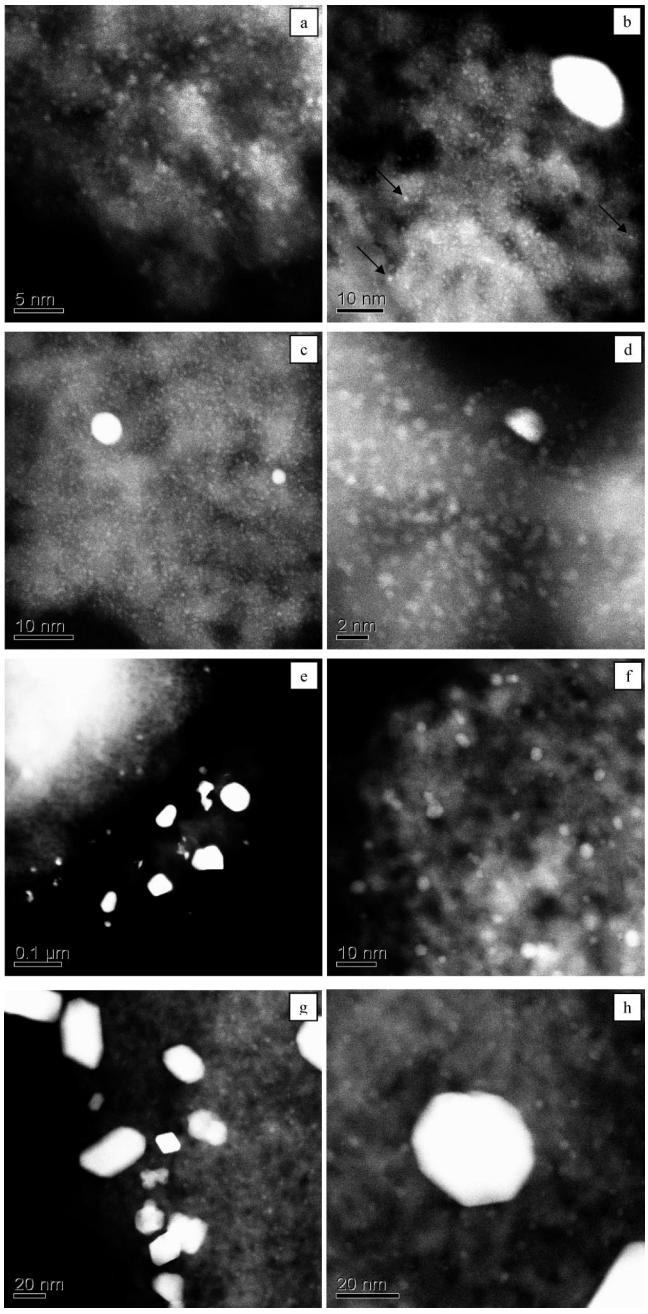

Figure 3. Representative STEM-HAADF images of the Au−Pd/Al_2O_3 catalysts: (a, b) uncalcined, (c, d) calcined at 200 °C, (e, f) calcined at 400 °C, and (g, h) calcined at 400 °C and reduced at 550 °C.

The particle size distribution remained, for the most part, unaffected after the catalyst calcined at 400 °C was subsequently reduced at 500 °C (Figure 3g,h) in that the reduced sample contained a large population of particles that were 20 nm or greater in diameter as well as the smaller 2–5 nm particles.

An experimental difficulty exists in quantitatively comparing the metal particle size distribution in the reduced sample relative to the catalyst that was only calcined at 400 °C. This is because the larger metal particles are not homogeneously distributed over the support surface, and therefore it was not feasible to accurately assess the relative number fractions that are present in the form of the smaller or larger particle populations. In turn, this makes it unrealistic to determine the difference in the overall metal dispersion between these two catalysts because subtle changes in the number fraction of the larger particles will significantly alter the particle size distribution in the catalyst. For example, a single 50 nm metal particle would contain approximately the same number of atoms as 15 000 particles with a diameter of 2 nm. Therefore, despite observing metal particles of very similar size in the calcined and reduced samples, a slight alteration to the particle size distribution in favor of the larger particles could significantly alter the total number of smaller particles present and result in a significant degradation of the catalyst performance.

3.3.2. STEM-XEDS Elemental Mapping of Au and Pd Spatial Distributions. (a) Uncalcined Au−Pd/Al_2O_3 Catalyst. STEM-XEDS mapping was utilized to further characterize the nature of the Au and Pd spatial distributions, which were found to be highly dependent upon the specific heat treatment used. For example, as the XEDS maps shown in Figure 4i indicate that a 15 nm particle analyzed in the uncalcined sample exhibited spatially coincident Au-M_α (Figure 4i.a) and Pd-L_α (Figure 4i.b) signals, suggesting that the Au−Pd particles within the uncalcined catalyst are homogeneous alloys with no observed Pd surface segregation. This is emphasized in the RGB reconstruction shown in Figure 4i.c. Semiquantitative analysis of this particle's composition suggests 72 wt % Au and 28 wt % Pd. In addition, the Pd signal detected in regions well away from the larger particles suggests that the sub-nanometer particles are highly Pd-rich. This is confirmed by extracting the XEDS data from 5 × 5 (i.e., 25) pixels corresponding to the "support" area (Figure 5a), in which Pd is detected but Au is not.

Finally, a tiny minority of the small (1–2 nm) particles, such as that shown in Figure 6a, were found and discovered to consist of pure Au. As shown in Figure 6b, the XEDS spectrum from the particle region shows no discernible Pd signal existing above the background noise. Interestingly, similar 2 nm, ostensibly pure Au particles were also observed in a previous investigation of an uncalcined Au−Pd/TiO_2 catalyst.[15] This could indeed explain the much brighter ADF contrast exhibited by some of the smaller particles (indicated with arrows in Figure 3b) relative to the majority of similarly sized particles. Because the image contrast from the different areas of the sample produced in the STEM-HAADF technique is highly dependent on the average atomic number, the brightest particles are most likely very Au rich compared to particles of similar size which produce lower contrast levels in these images.

(b) Au−Pd/Al_2O_3 Catalyst Calcined at 200 °C. After the fresh catalyst was calcined at 200 °C, representative STEM-XEDS data from a 22 nm particle presented in Figure 4ii shows that the X-ray maps of the Au-M_α (Figure 4ii.a) and Pd-L_α (Figure 4ii,b) signals no longer occupy the same spatial area, as in the uncalcined catalyst. Instead, the Pd signal originates from a slightly larger projected area than that of the Au, suggesting that a slight surface enrichment of Pd has occurred during the heat treatment. This particular particle was found to be more Au-rich (87 wt %) than that measured in the uncalcined sample. Also, while the signal produced by the Pd dispersed over the Al_2O_3 support surface

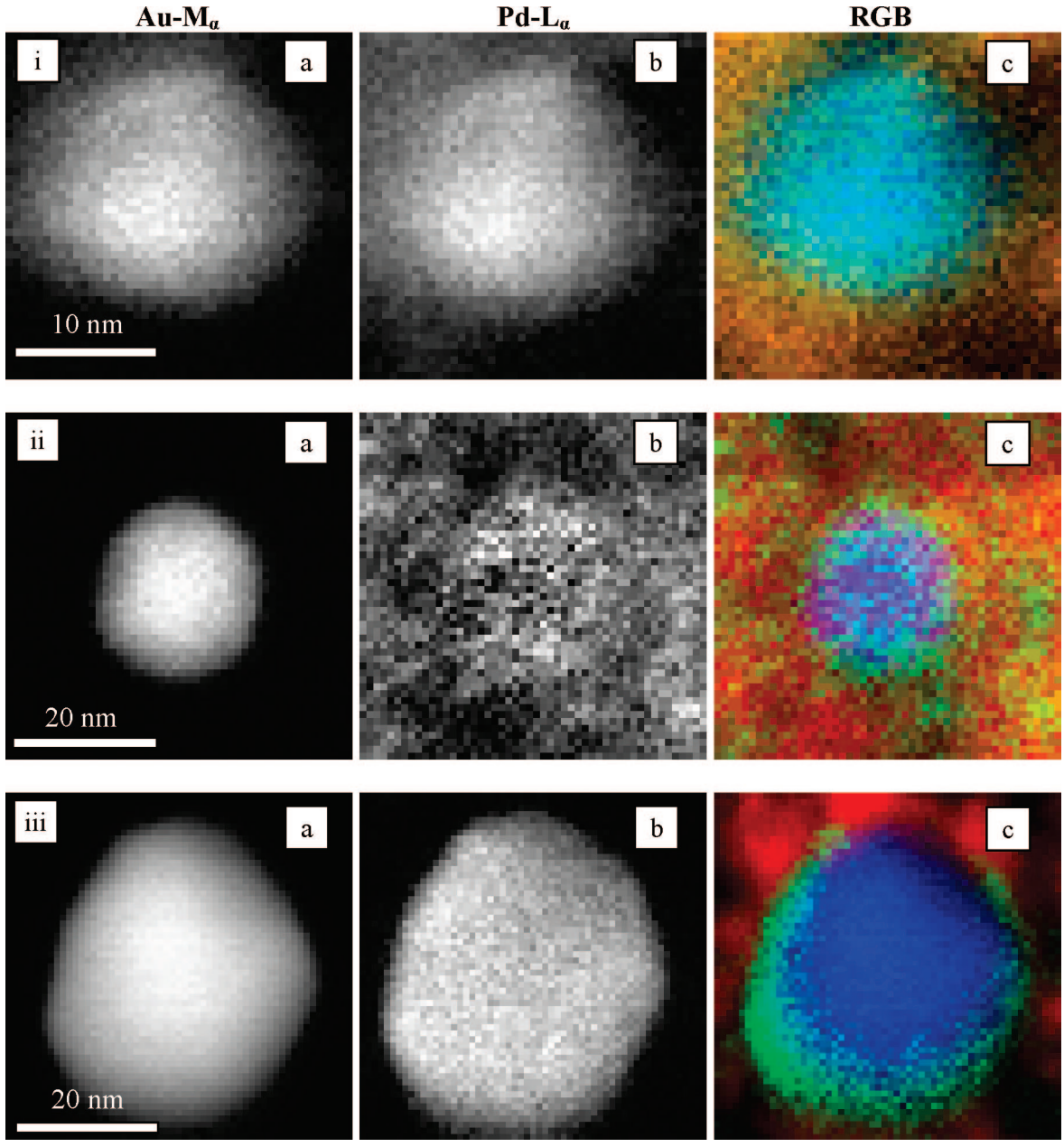

Figure 4. Montage of STEM-XEDS data from Au−Pd/Al_2O_3 catalysts at various heat treatments. (i) Uncalcined, (ii) calcined at 200 °C, and (iii) calcined at 400 °C. (a) Au-M_α, (b) Pd-L_α, and (c) RGB reconstruction where red = Al, green = Pd, and blue = Au.

is still significant (Figure 5b), it is considerably weaker than that observed in the uncalcined sample. This suggests that the highly dispersed Pd species, which was prevalent in the uncalcined catalyst, had begun to sinter during the calcination treatment. Finally, it should be noted that the small, pure-Au particles observed in the uncalcined sample were not found at all in the sample calcined at 200 °C, which is consistent with the similar contrast exhibited in the STEM-HAADF image (Figure 3c,d) by all of the 2–5 nm metal particles in this sample. This last observation must be slightly qualified since the frequency of observation of the 2–5 nm Au-rich particles in the uncalcined catalyst was so low, they might have existed in the catalyst calcined at 200 °C but were not detected in the population sampled.

(c) Au−Pd/Al_2O_3 Catalyst Calcined at 400 °C. After calcination at 400 °C STEM-XEDS analysis showed that the Au−Pd core–shell morphology was routinely exhibited by the larger metal particles in the catalyst. The elemental maps obtained from a 30 nm particle, shown in Figure 4iii, indicate that the Au-M_α signal (Figure 4iii.a) originates from a much smaller spatial area than that of Pd-L_α (Figure 4iii.b). The core–shell structure is also indicated by the drop in intensity of the Pd-L_α signal at the center of the particle relative to the perimeter, which is the opposite trend to that seen in the Au signal. This particular particle exhibited a similar Au-rich (89 wt %) composition to the particle analyzed in the sample calcined at 200 °C. In addition, when contrasted with comparable data from the previous two samples, the XEDS spectra extracted from the "support" area (Figure 5c) in this catalyst contained no discernible Pd component, indicating that most of the highly dispersed Pd species had now been incorporated into the particles which were greater than 2 nm in diameter during this elevated temperature heat treatment.

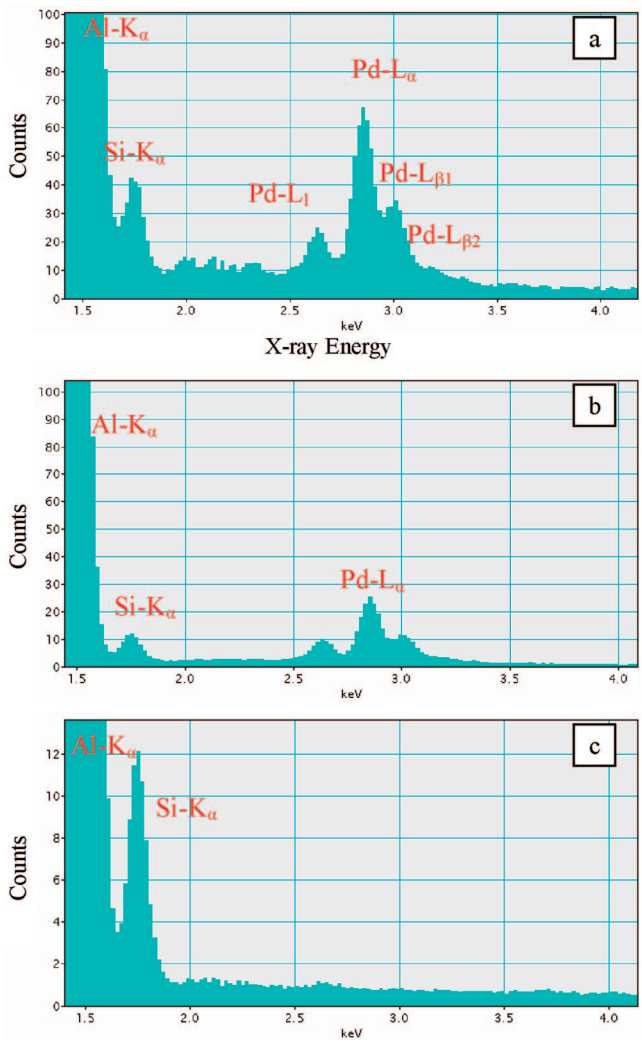

Figure 5. XEDS spectra extracted from 5 × 5 (i.e., 25) pixels corresponding to the "support" area in the STEM spectrum image acquired from the Au−Pd/Al_2O_3 catalysts. (a) uncalcined, (b) calcined at 200 °C, and (c) calcined at 400 °C. Note the progressive decrease in the amount of Pd detected on the support surface as the calcination temperature is increased.

(d) Au−Pd/Al_2O_3 Catalyst Calcined at 400 °C and Subsequently Reduced at 500 °C. Subsequent STEM-XEDS analysis was carried out on the particles designated in the ADF images presented in Supporting Information, Figure 1. The results of this analysis, shown in Figure 7, indicated that the distributions of the Au and Pd within the particles varied significantly from particle to particle. For example, the Pd-rich shell/Au-rich core morphology that was observed in the catalyst calcined at 400 °C was again observed in the reduced sample, as shown in the XEDS maps in Figure 7i,ii. Indeed, the shell thickness in these particles appears to be even larger than observed in the catalyst calcined at 400 °C, though the analysis of the exact same particle both before and after calcination is not possible so this statement must be slightly qualified. In contrast, other particles observed (Figure 7iii,iv) in the reduced sample exhibited an inversion of this core–shell morphology so that the surface was significantly Au-rich and the core was Pd-rich. This observation may help explain the fact that the Au(4f) peak intensity increases on reduction relative to the Pd(3d) peak intensity (Table 1). Therefore, in these latter particles, the reduction treatment has had the effect of reversing the core–shell morphology seen in the catalyst calcined at 400 °C.

Finally, semiquantitative compositions of the Au−Pd particles in this reduced sample (Figure 7) do not indicate that there is any compositional dependence on whether the core–shell morphology inversion occurs. Caution should be used, however, as the error in these compositional values is likely to be high because a standardless, Cliff−Lorimer type quantification procedure was employed using theoretical k-factor values.

4. Discussion

To summarize, a systematic series of Au−Pd/Al_2O_3 catalysts has been investigated in an effort to characterize the evolution of particle composition and structure during various heat treatments and their correlation with catalytic performance for the H_2 and O_2 direct combination reaction. Fresh, uncalcined Au−Pd catalysts were found to be complex systems consisting of highly dispersed sub-nanometer Pd species, 2 nm pure Au particles, and occasional larger, homogeneous alloy particles. After calcination, the particles began to exhibit surface enrichment of Pd, and sintering of the highly dispersed Pd on the support surface occurred, both of these effects becoming more pronounced with increasing calcination temperature. In many particles, the Au-rich core/Pd-rich shell morphology is retained even after a subsequent reduction treatment; however, a significant fraction of particles exhibiting the reverse morphology (i.e., Pd-rich core, Au-rich shell) were also observed. The sintering of the metal particles and/or the surface segregation of Pd during the heat treatments is deleterious to the H_2O_2 production values exhibited by these materials; however, calcination is necessary to produce a stable and reusable catalyst because significant leaching of the metal from the fresh sample and the sample calcined at 200 °C occurs during reaction.

These experiments clearly indicate that the Au-rich core/Pd-rich shell morphology is formed during the calcination treatments and that the degree of segregation and extent of the shell thickness increases with temperature. Thermodynamic considerations suggest that such Pd surface enrichment is not an equilibrium process in the Au−Pd system. Instead, the binary phase diagram predicts that an face-centered cubic solid solution of Au and Pd is formed over the entire compositional range with special ordering compounds existing at the Au_3Pd and $AuPd_3$ compositions.[26] It should also be noted that a third ordered phase is possible at 35 wt % Pd (i.e., at a 1:1 Au−Pd atomic ratio), although this alloy structure has been poorly characterized. Furthermore, molecular dynamics simulations performed by Liu et al.[27] predict that the Au-core/Pd-shell structure is only stable at very low temperature and should rapidly change to the energetically favorable Pd-rich core/Au-rich shell morphology at higher temperatures. Simple surface energetics also predict that Au would be the favored surface material in a

(26) Okamoto, H.; Massalski, T. B. *Phase Diagrams of Binary Gold Alloys*; ASM International: Metals Park, OH, 1987.
(27) Liu, H. B.; Pal, U.; Medina, A.; Maldonado, C.; Ascencio, J. A. *Phys. Rev. B* **2005**, *71*, 075403.

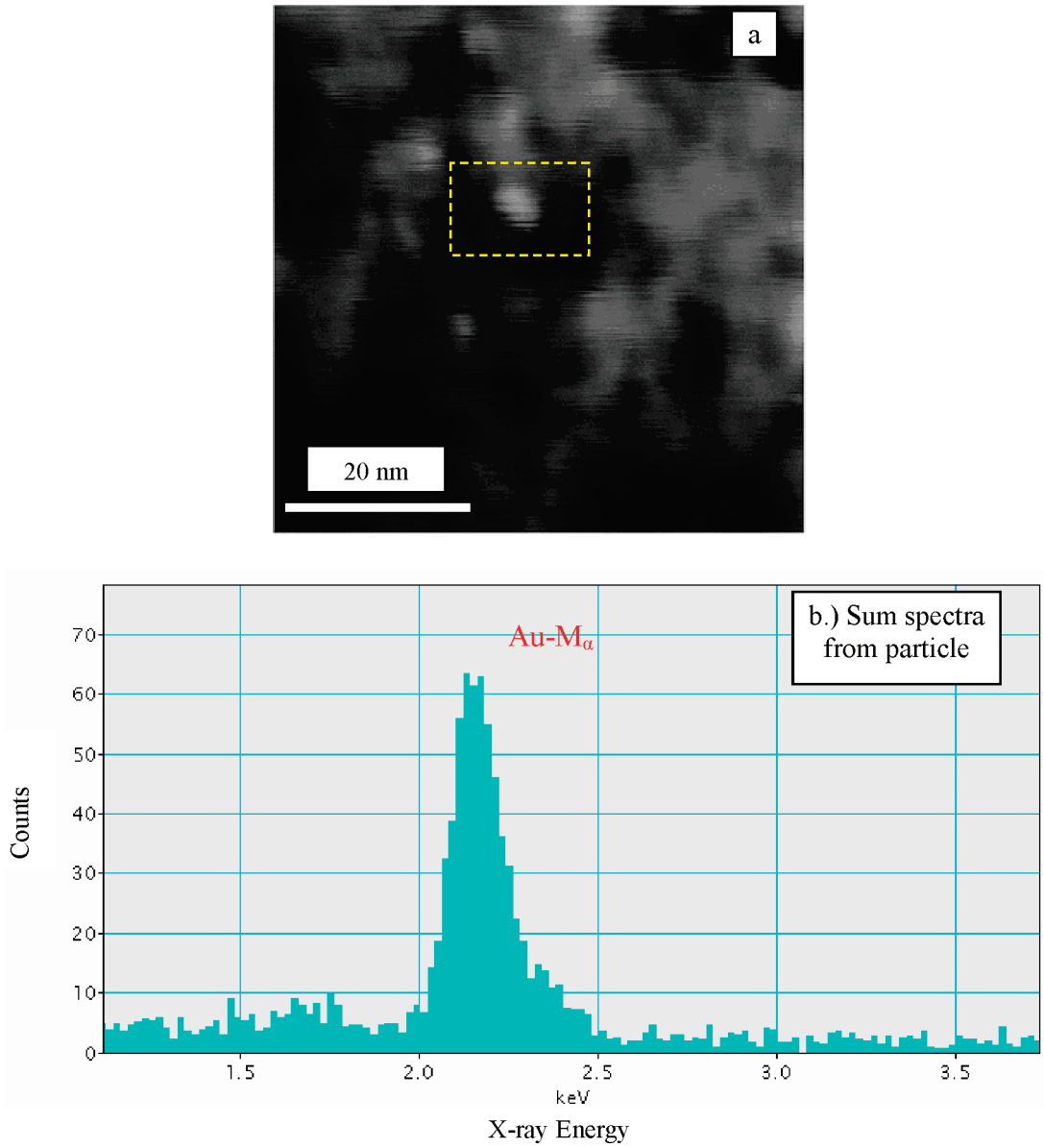

Figure 6. (a) ADF image acquired using the VG HB603 STEM and (b) the corresponding sum spectra extracted from the MSA-processed spectrum image pixels associated with the metal particle.

core–shell particle since the surface energies of Au and Pd are 1.50 and 2.05 J/m^2, respectively.[28]

However, similar surface segregation in bimetallic catalyst systems such as Pt−Rh have been previously reported.[29] Also, Hilaire et al.[30] have observed similar surface segregation of Pd in bulk Au−Pd alloys, and this effect has been ascribed to migration of Pd atoms, which are more easily oxidized at the calcination temperature, to the metal surface to form Pd−O bonds. In addition, it was found that the oxidized surface of Pd could be converted to Pd metal by a subsequent reduction treatment without a corresponding re-equilibration of the alloy composition. In other words, the surface can remain enriched with Pd despite the removal of the oxygen, which initiated its segregation in the first place. Again, this correlates well with the XPS analysis which indicated that the Pd was fully reduced to Pd^0 following the heat treatment in flowing H_2.

The results presented here agree well with the development of the core–shell morphology in the Au−Pd nanoparticles in the present study. While the uncalcined sample exhibited particles that were homogeneous alloys, the calcination treatment at 200 °C initiated migration of Pd to the surface. The increased diffusion rates expected at calcination temperatures of 400 °C result in a greater degree of segregation for a similar heat treatment time. The present XPS analysis also matches the bulk observations of Hilaire et al. [30] since it showed that the surface Pd in the Al_2O_3 catalysts existed in a Pd^{2+} valence state in the as-synthesized sample (most likely as $PdCl_2$) and remains as such throughout the elevated temperature calcination treatments after it is converted to PdO.

(28) de Boer, F. R.; Boom, R.; Mattens, W. C. R.; Miedema, A. R.; Niessen, A. K. *Cohesion in Metals*; North Holland: Amsterdam, 1988.
(29) Lyman, C. E.; Hepburn, J. S.; Stenger, H. G. *Ultramicroscopy* **1990**, *34*, 73.
(30) Hilaire, L.; Legare, P.; Holl, Y.; Maire, G. *Surf. Sci.* **1981**, *103*, 125.

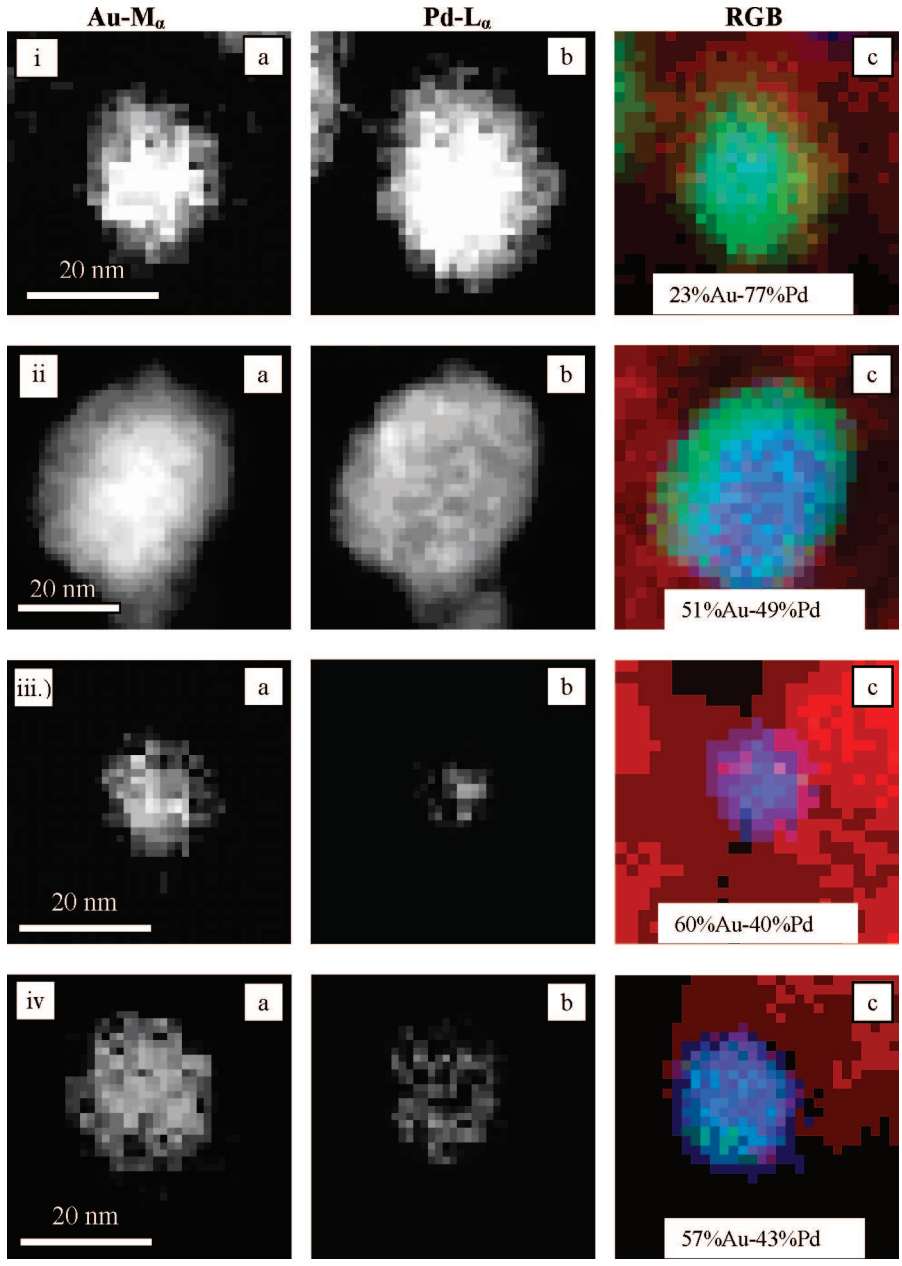

Figure 7. Representative STEM-XEDS maps and RGB reconstructions for the Au-M_α and Pd-L_α signals of the Au−Pd/Al_2O_3 catalysts calcined at 400 °C and reduced at 500 °C (red = Al, green = Pd, and blue = Au). Au-rich core/Pd-rich shell particles (a and b) and the opposite (c and d) Pd-rich core and Au-rich shell are clearly shown.

The XPS results obtained from the catalyst that was calcined at 400 °C and subsequently reduced in H_2 indicated that the Pd was fully reduced to Pd^0 following this treatment, and the STEM-XEDS data showed that some of the particles retained the Au-rich core/Pd-rich shell morphology. This agrees well with work reported for bulk alloys,[30] where Pd surface-enrichment could be retained even after the PdO was reduced in flowing H_2. However, the previous study did not report any data that would have allowed us to predict the tendency of some of the particles in the Au−Pd/Al_2O_3 catalysts to "turn inside-out" (i.e., to form a Pd-rich core/Au-rich shell morphology) as discovered in the present study. It is tempting to attribute this core–shell inversion phenomenon to the reduction in surface energy of the particle by its adoption of an Au-rich, rather than Pd-rich, surface,[28] which would also agree with the equilibrium structure predicted by molecular dynamics.[27] However, this explanation fails to take into account the large number of particles that retain their original Au-rich core/Pd-rich shell morphology even after the elevated temperature reduction.

It should be noted that the particles that were analyzed via STEM-XEDS to track these morphological developments were all much larger than the majority of the particles present in the samples. This was necessary because detecting surface segregation in the smaller (1–5 nm) particles is extremely difficult since the shell thickness decreases proportionately with particle size. A simple geometrical calculation involving a hemispherical particle that exhibits total segregation (i.e., all of the Pd in the particle migrates to the surface and the core consists of pure Au) shows that the ratio of the shell thickness to the particle radius would equal 0.206. Therefore, for particles of 15 and 5 nm in diameter, the shell thicknesses

become 1.54 and 0.52 nm, respectively. This makes the detection of surface segregation in particles smaller than ~15 nm extremely difficult. However, when the STEM-XEDS analysis of these larger particles is coupled with particle size measurements and XPS data it can be inferred that these same changes are occurring in the more plentiful 1–5 nm particles simultaneously.

4. Conclusions

A series of $Au-Pd/Al_2O_3$ catalysts was synthesized using a variety of heat treatments, and STEM-XEDS and XPS analyses were utilized to track the morphological development of the bimetallic particles. It was found that Au-rich core/Pd-rich shell particles developed during calcination treatments, the process being driven by the preferential oxidation of Pd relative to Au at the heat treatment temperatures. Subsequent reduction of a previously calcined catalyst caused many of the particles to invert and form Pd-rich core/Au-rich shell morphologies, while others retained their original Pd surface enrichment. The development of phase segregated particles during the heat treatments was accompanied by particle sintering and a decrease in catalytic performance for H_2O_2 production. However, this calcination step cannot be avoided because it is crucial to produce a stable, reusable catalyst.

Acknowledgment. This work formed part of the EU AURICAT project (Contract No. HPRN-CT-2002-00174) and the ATHENA project sponsored by the EPSRC and Johnson Matthey PLC, and we thank them for funding this research. We also thank the World Gold Council, for providing funding under the GROW scheme, and Cardiff University for the award of an AA Reed studentship to J.K.E. A.A.H. and C.J.K. acknowledge the generous support of NSF Materials Research Science and Engineering Center (NSF DMR 0079996).

Supporting Information Available: STEM-ADF images acquired using the VG HB603 STEM of the $Au-Pd/Al_2O_3$ catalyst calcined at 400 °C and subsequently reduced at 500 °C. and relative Au^{x+}/Au^0 and normalized Cl contents of the $Au-Pd/Al_2O_3$ catalysts as determined via XPS analysis. This material is available free of charge via the Internet at http://pubs.acs.org.

CM702762D